

**Project PAJex1
Report No2**

**Comparison of the
Measured and Predicted
Deformation of an
Adhesively Bonded
Lap-Joint Specimen**

G Dean & L Crocker

November 2000

© Crown copyright 2000
Reproduced by permission of the Controller of HMSO

ISSN 1361-4061

National Physical Laboratory
Teddington, Middlesex, UK, TW11 0LW

Extracts from this report may be reproduced provided the source is
acknowledged and the extract is not taken out of context.

Approved on behalf of Managing Director, NPL, by Dr C Lea,
Head, Centre for Materials Measurement and Technology

CONTENTS

1	<u>INTRODUCTION</u>	1
2	<u>MATERIAL</u>	2
3	<u>DETERMINATION OF MATERIALS PROPERTIES</u>	3
3.1	<u>TESTS ON BULK SPECIMENS</u>	3
3.2	<u>MATERIALS MODELS</u>	3
3.3	<u>DETERMINATION OF DATA FOR EACH MODEL</u>	6
3.3.1	<i>Elastic properties</i>	6
3.3.2	<i>The strain hardening function $\mathbf{s}_T(\mathbf{e}_p)$</i>	6
3.3.3	<i>Hydrostatic stress sensitivity parameters $\tan \mathbf{b}$ and \mathbf{a}</i>	6
3.3.4	<i>The flow parameter $\tan \mathbf{y}$</i>	8
3.3.5	<i>Rate-dependent hardening functions $\sigma_T(\epsilon_p, \dot{\epsilon}_p)$</i>	8
4	<u>FINITE ELEMENT ANALYSIS OF JOINT PERFORMANCE</u>	11
4.1	<u>SPECIMEN GEOMETRY</u>	11
4.2	<u>QUASI-STATIC ANALYSIS</u>	12
4.3	<u>DYNAMIC ANALYSIS</u>	13
4.3.1	<i>Explicit versus Implicit Analysis</i>	13
4.3.2	<i>Analysis with Rate-Dependent Adhesive Properties</i>	14
4.4	<u>STRAIN CALCULATIONS</u>	16
5	<u>EXPERIMENTAL TESTS ON THE LAP-JOINT SPECIMENS</u>	17
6	<u>EVALUATION OF A FAILURE CRITERION</u>	17
7	<u>COMPARISON OF MEASURED AND PREDICTED JOINT PERFORMANCE</u>	19
7.1	<u>FORCE/EXTENSION BEHAVIOUR</u>	19
7.2	<u>EVALUATION OF THE FAILURE CRITERION</u>	20
8	<u>CONCLUSIONS AND FURTHER WORK</u>	22
9	<u>ACKNOWLEDGEMENTS</u>	23

Comparison of the Measured and Predicted Deformation of an Adhesively Bonded Lap-Joint Specimen

G Dean and L Crocker

Centre for Materials Measurement and Technology and
National Physical Laboratory,
Teddington, Middlesex TW11 0LW

SUMMARY

Force versus extension curves and strain distributions for a lap-joint specimen have been calculated using finite element analyses. The specimen is bonded using a modern rubber toughened adhesive chosen for its high toughness. Calculations have been made over a range of loading speeds using the linear and exponent Drucker-Prager materials models. The measurement and analysis of experimental data needed to derive the materials parameters and properties required for the predictions are described. Particular attention has been given to the acquisition of data at high strain rates that are relevant for predictions of performance under impact.

The predicted force/extension curves are compared with measured data and are seen to lie at consistently higher force levels for each loading speed. An explanation for this is proposed associated with the progressive rupture of the adhesive layer under load. This explanation is supported by the results of failure measurements on bulk and butt-joint specimens of the adhesive and calculations of strain distributions in the adhesive before and after the onset of rupture.

1 INTRODUCTION

One of the main objectives of Project PAJ2 in the previous Adhesives Programme was to establish how finite element methods can be used most effectively to predict the performance of an adhesive joint under different speeds of loading including impact. Of interest here was the accuracy with which force/extension curves and joint rupture could be predicted. Calculations of the performance of a lap-joint specimen were made using three elastic-plastic materials models that were based on different yield criteria. These gave slightly different predictions of the force/extension curve at a particular speed but relatively large differences in the level of strain in the region of strain concentration where joint failure is expected to initiate. In another part of the project, a failure criterion was proposed (1) which stated that adhesive rupture occurs at a critical level of strain which was dependent on the strain state (the relative proportion of shear and dilatational strain). The importance of the ability of the analysis to make accurate predictions of strain is therefore evident. In order to explore the accuracy that can be achieved in predictions of deformation and failure, calculations were compared with measurements made on lap joint specimens of a new toughened epoxy LMD1142 supplied by Ciba. The properties of the adhesive required by the FE analyses were obtained from tests on bulk specimens of the adhesive (2). These were measured over a wide range of strain rates in the specimen so that predictions of joint performance could be made at different loading speeds (3).

On comparing measured and predicted results (3), it was observed that the calculated peak force at each loading speed was consistently higher than measured values. The response at lower extensions, where behaviour is predominantly elastic, was accurately predicted.

In an attempt to explain this lack of agreement between measured and calculated performance, the possibility was investigated of local, but not catastrophic failure occurring in the adhesive at sites of strain concentration. It was considered that if rupture occurred in these local regions, then the joint would be weakened in comparison with the undamaged state assumed by the analysis. However, the analyses revealed that the maximum strain in the adhesive at the extension at which the measured and predicted force/extension curves started to depart was significantly below the strain level at

which rupture could be expected from the results of tensile tests on bulk and butt-joint specimens (1).

Although the possibility of local premature failure could not be totally discounted, it was concluded that the most probable reason for the discrepancy between measurement and prediction was that the properties of the bulk adhesive, from which the data for the FE analysis were obtained, were different from those of the thin layer of adhesive in the bonded joint. Although this was not an obvious conclusion in the light of earlier studies comparing bulk and joint properties (4), it was plausible in this case since the adhesive was an experimental grade with a novel structure of the toughening phase. It was thus considered feasible that the structure of this phase could be sensitive to curing conditions, the thickness of the adhesive and the presence of adherend surfaces.

In the work reported here, comparisons have been made between the measured and predicted performance of the lap-joint specimen using a different toughened epoxy adhesive. Prior tests have revealed that data derived from bulk specimens should be representative of the adhesive in a bonded joint. The results of the work allow a further evaluation of the failure criterion (1) proposed in the previous project.

2 MATERIAL

The adhesive chosen for this study was a one part, toughened epoxy supplied by Gurit Essex. Bulk specimens were cut from sheets of 3 mm nominal thickness prepared using procedures described in earlier work (3). Butt-joint and lap-joint specimens had a thickness of 0.5 mm. The bulk specimen sheets were placed in an oven that had been pre-heated to 180 °C and were cured for a period of 1 hour after which the oven was switched off. The joint specimens were surrounded by a joint alignment frame and, because of the greater mass of metal, were allowed to cure for a period of 90 minutes before the oven was switched off.

In order to investigate the influence of specimen thickness and cure time on material properties, bulk specimen sheets were prepared ranging in thickness between 1 mm and 3 mm. These were cured at two rates corresponding to those used for the bulk and joint specimen preparation referred to above.

3 DETERMINATION OF MATERIALS PROPERTIES

3.1 TESTS ON BULK SPECIMENS

The properties of the epoxy adhesive required for finite element analyses have been determined from tensile and shear tests on bulk specimens. These methods are described in reference (2). In order to gain some support for using bulk specimen data to represent the properties of the adhesive in a bonded joint, some preliminary tensile tests were carried out on specimens of different thickness, prepared using different cure times. Bulk specimen sheets were moulded having thicknesses of 1 mm and 3 mm. The thinner sheets were cured at the rate used to prepare joint specimens. Some of the thicker sheets were also cured at this rate whilst other sheets were cured at the faster rate used for bulk specimen preparation. The results of tensile tests carried out on specimens cut from these sheets are shown in figure 1. These show that the reproducibility in stress/strain behaviour is very good and that tensile properties are insensitive to cure conditions and specimen thickness.

3.2 MATERIALS MODELS

The epoxy adhesive is a ductile material that exhibits yielding and plastic flow in tension before failure at a tensile strain of about 0.1. Elastic-plastic models have therefore been used to describe the deformation behaviour of the adhesive for finite element analyses. FE analyses have been carried out using three models which differ in the form of the yield criterion. With each of these models, the elastic behaviour is characterised by values for the Young's modulus E and the Poisson's ratio ν_e .

The simplest elastic-plastic model is based on the von Mises yield criterion

$$\sigma_T = \sqrt{3} J_{2D}^{1/2} = q \quad (1)$$

where σ_T is a yield stress in tension and is a material property. $J_{2D}^{1/2}$ is an invariant of the deviatoric stress tensor and is a measure of the effective shear stress applied to the material and q is the terminology used in ABAQUS to represent this effective shear stress. Adhesives strain harden after the onset of yield so σ_T is a function of plastic strain ϵ_p . The function $\sigma_T(\epsilon_p)$ is the strain-hardening function and is required by the analysis.

It is known that the von Mises criterion is not an accurate description of yielding in adhesives since plasticity is sensitive to the hydrostatic as well as the shear component of stress. The simplest yield criterion that includes hydrostatic stress sensitivity is a modification of equation (1) as follows

$$\sigma_T = \frac{\sqrt{3}(\lambda + 1)}{2\lambda} J_{2D}^{1/2} + \frac{(\lambda - 1)}{2\lambda} J_1 \quad (2)$$

Here J_1 is the first invariant of the stress tensor and is equal to 3 times the hydrostatic component of stress. The parameter λ is a measure of the sensitivity of yielding to the hydrostatic stress and is equal to the ratio of yield stresses in compression and tension at the same equivalent plastic strain. In ABAQUS, this criterion is used in the linear Drucker-Prager model and takes the form

$$d = q - p \tan \beta \quad (3)$$

where

$$d = \frac{2\lambda\sigma_T}{(\lambda + 1)}, \quad \tan \beta = \frac{3(\lambda - 1)}{(\lambda + 1)} \quad \text{and} \quad p = -\frac{J_1}{3}$$

Since $\tan \beta$ is to be determined from measurements of tensile and shear yield stresses, it follows from equation (3) that

$$\tan \beta = 3 \left(\frac{\sqrt{3}\sigma_s}{\sigma_T} - 1 \right) \quad (4)$$

where σ_s and σ_T are yield stresses obtained at the same effective plastic strain (see section 3.3.3).

A flow parameter ψ is also required for this model. This is calculated from measurements of the plastic component of Poisson's ratio ν_p and is given by

$$\tan \psi = \frac{3(1 - 2\nu_p)}{2(1 + \nu_p)} \quad (5)$$

If $\tan \psi = \tan \beta$ then the flow is associated.

An alternative yield criterion that is sensitive to the hydrostatic stress is

$$\lambda \sigma_T^2 = 3J_{2D} + (\lambda - 1)\sigma_T J_1 \quad (6)$$

In ABAQUS, this criterion is used in the exponent Drucker-Prager model and is described by the equation

$$a q^2 = p + p_t \quad (7)$$

where $a = \frac{1}{3\sigma_T(\lambda - 1)}$ and $p_t = a \lambda \sigma_T^2$

It follows from equation (6) that

$$a = \frac{\sigma_T}{3(3\sigma_s^2 - \sigma_T^2)} \quad (8)$$

where, once again, σ_T and σ_s relate to the same effective plastic strain (see section 3.3.3).

3.3 DETERMINATION OF DATA FOR EACH MODEL

3.3.1 Elastic properties

The Young's modulus E and the elastic component of Poisson's ratio ν_e were determined from measurements of stress, longitudinal strain and the lateral strain in tensile tests on bulk specimens at small strains where the stress/strain plot is linear. Values for Young's modulus were observed to increase very slightly with strain rate. Values at a strain rate of $2 \cdot 10^{-3} \text{ s}^{-1}$ are shown in table 1.

Table 1 – Properties of the epoxy adhesive used for finite element analyses

E (GPa)	ν_e	$\tan \beta$	a (MPa^{-1})	ν_p	$\tan \psi$	$\sigma_T(\epsilon_p)$ (MPa)
2.97	0.35	0.82	0.009	0.27	0.54	see fig 3

3.3.2 The strain hardening function $\sigma_T(\epsilon_p)$

Figure 2 shows true stress/true strain curves measured in tension and shear on bulk specimens. Test speeds were chosen so that the effective plastic strain rate $\dot{\epsilon}_p$ (see section 3.3.3) was the same in both tests. The hardening function for tensile behaviour is obtained from the tensile curve in figure 2 by subtracting the elastic strain component from each value of the total tensile strain. The resulting hardening curve is presented in figure 3 as a plot of true stress (now the yield stress) against true plastic strain.

3.3.3 Hydrostatic stress sensitivity parameters $\tan \beta$ and a

The parameters that characterise the hydrostatic stress sensitivity of plastic deformation, $\tan \beta$ for the linear Drucker-Prager model and a for the exponent Drucker-Prager model, were determined

from tensile and shear yield stresses using equations (4) and (8). The yield stresses σ_T and σ_S in these equations need to be determined at the same effective plastic strain $\bar{\epsilon}_p$ and effective plastic strain rate $\dot{\bar{\epsilon}}_p$. The definition of effective plastic strain used here for the determination of model parameters is based on von Mises yielding. Thus

$$\bar{\epsilon}_p = \frac{2I_{2D}^{1/2}}{\sqrt{3}} \quad (9)$$

where

$$I_{2D}^{1/2} = \left\{ \frac{1}{6} [(\epsilon_{p1} - \epsilon_{p2})^2 + (\epsilon_{p2} - \epsilon_{p3})^2 + (\epsilon_{p3} - \epsilon_{p1})^2] \right\}^{1/2}$$

and ϵ_{p1} , ϵ_{p2} and ϵ_{p3} are components of principal plastic strain. It follows that under uniaxial tension

$$\bar{\epsilon}_p = \epsilon_{pT}, \text{ the plastic tensile strain} \quad (10)$$

and in shear

$$\bar{\epsilon}_p = \frac{\gamma_p}{\sqrt{3}} \quad (11)$$

where γ_p is the plastic component of the engineering shear strain and is equal to 2x the plastic component of the tensor shear strain. Similarly, the effective yield stress $\bar{\sigma}$ is given by the expression

$$\bar{\sigma} = \sqrt{3} J_{2D}^{1/2} = q \quad (12)$$

so that in tension

$$\bar{\sigma} = \sigma_T, \text{ the tensile yield stress} \quad (13)$$

and in shear

$$\bar{\sigma} = \sqrt{3} \sigma_S \quad (14)$$

Using equations (10) to (14), the measured stress/strain curves in tension and shear shown in figure 2 have been plotted on axes of effective stress against effective plastic strain in figure 3. In this way, values for $\sqrt{3} \sigma_S$ and σ_T can be readily selected at the same effective strain. This plot also shows the departure of the yield behaviour of this adhesive from the von Mises criterion. For a von Mises material, the two curves would coincide.

Using the results in figure 3 with equation (4) gives values for $\tan \beta$ that rise with plastic strain to a constant value of 0.82 at plastic strains above 0.03 as recorded in table 1. Using equation (8) with the data in figure 3 gives a value for a of 0.009.

3.3.4 The flow parameter $\tan \psi$

Results for the measured Poissons ratio of the adhesive obtained from a tensile test are shown in figure 2. From these results, the plastic component v_p was calculated. A mean value for $v_p = 0.27$ was used to calculate the flow parameter using equation (5), and these values are recorded in table 1.

3.3.5 Rate-dependent hardening functions $\sigma_T(\epsilon_p, \dot{\epsilon}_p)$

With the parameters in table 1, it is possible to use finite element methods to calculate the deformation of a joint at a speed such that the effective strain rate in the adhesive is equal to the strain rate pertaining to the test data used to derive these parameters (in this case 0.002 s^{-1}). In order to calculate the behaviour at specified speeds, the dependence of properties on strain rate is

required. The main rate-dependent property is the hardening function $\sigma_T(\epsilon_p)$. The other parameters show very small dependencies upon strain rate which are difficult to measure and cannot be taken into account in the FE analysis.

Rate dependent hardening functions can be obtained from measurements of stress/strain curves in tension at different test speeds. Results for the epoxy adhesive are shown in figure 4 spanning a range of plastic strain rate from $2 \cdot 10^{-4} \text{ s}^{-1}$ to 40 s^{-1} . Tests were carried out at constant cross-head speed. A variety of methods was used to measure the strain in these tests as described in a previous report (5). The strain rates recorded with the data are mean values of the plastic strain rate which is effectively constant during a test. From these data, yield stress/plastic strain curves were derived and are shown in figure 5.

In order to predict joint performance at speeds up to 1 m/s, it is necessary to extend the strain rate range for these data by a factor of about 100. For this purpose, the hardening curves in figure 5 have been modelled using an empirical function. The function used is

$$\sigma_T = \left[\sigma_o + (\sigma_f - \sigma_o) (1 - \exp -(\epsilon_p / \epsilon_{ps})^n) \right] (1 + \alpha \epsilon_p) \quad (15)$$

With this curve, yield stresses σ_T increase from σ_o (the first yield stress) corresponding to zero plastic strain to a value of σ_f (the initial flow stress) corresponding approximately to the plateau stress. The parameter ϵ_{ps} represents some mean strain where the stress is rising rapidly between σ_o and σ_f , and the parameter n influences the strain range over which the rise in stress occurs. The term containing the parameter α describes a small increase of σ_T with plastic strain during flow. Values for these parameters giving the best fit of equation (15) to the data in figure 5 are shown in table 2. It can be seen from this table that the main strain rate dependence occurs in the parameters σ_o and σ_f . The parameters ϵ_{ps} , n and α are essentially rate independent for this material and can be assumed to take average values of 0.005, 0.6 and 0.85 without significant loss of predictive accuracy.

Table 2 – Values for the parameters in equation (15) giving the fits shown to the data in figure 5

$\dot{\epsilon}_p$ (s ⁻¹)	0.0002	0.002	0.026	0.25	1.1	41
σ_o (MPa)	16	18	20	20	22	24
σ_f (MPa)	52	58	65	73	81	90
ϵ_{ps} (s ⁻¹)	0.003	0.004	0.005	0.005	0.006	0.005
n	0.6	0.6	0.6	0.6	0.6	0.55
α	0.7	0.7	1	0.7	0.85	0.85

The variation of the yield stress of plastics with strain rate is usually described using the Eyring equation which can be expressed as

$$\sigma_y = A + B \log \dot{\epsilon}_p$$

Here σ_y is generally taken as the peak stress in a stress/strain curve measured at the strain rate $\dot{\epsilon}_p$. A and B are temperature-dependent materials parameters. The yield stress parameters σ_o and σ_f in equation (15) have accordingly been modelled using the equations

$$\sigma_f = \sigma_{fo} (1 + b \log \dot{\epsilon}_p) \quad (16)$$

$$\sigma_o = \sigma_{oo} (1 + c \log \dot{\epsilon}_p)$$

Plots of σ_f and σ_o taken from Table 2 against $\log \dot{\epsilon}_p$ are shown in figure 6. Equations (16) give satisfactory fits to the data and yield values for $\sigma_{fo} = 78$ MPa, $\sigma_{oo} = 21.5$ MPa, $b = 0.041$ and $c = 0.028$.

The derived values for the parameters in equations (15) and (16) are presented in table 3. Hardening curves predicted using these parameters are compared with experimental data in figure 7.

The fits to the data are seen to be satisfactory. Also shown are predicted curves at strain rates of 250 s^{-1} and 2500 s^{-1} which are beyond the strain rate for which accurate measurements are possible. These curves have been used to calculate the performance of the lap-joint specimen at different loading speeds as described in the next section.

**Table 3 – Values for the parameters in equations (15) and (16)
used to model rate-dependent hardening curves for
the epoxy adhesive**

σ_{i0} (MPa)	σ_{00} (MPa)	b	c	ϵ_{ps} (s^{-1})	n	α
78	21.5	0.041	0.028	0.005	0.6	0.85

4 FINITE ELEMENT ANALYSIS OF JOINT PERFORMANCE

4.1 SPECIMEN GEOMETRY

A lap shear test specimen was chosen for the comparison of measured and predicted joint behaviour. A diagram showing the geometry and dimensions of the specimen is shown in figure 8. To improve the accuracy of strain predictions in the region of maximum strain in the adhesive, geometric singularities have been removed by incorporating a radius on the edges at the end of each adherend, and a circular fillet on each end of the adhesive.

The lapjoint was meshed using the pre-processor FEMGV. The ABAQUS continuum 2-D solid plane strain elements (CPE4R) were used. Preliminary results were obtained using the mesh shown in figure 9. Mesh density can affect the strain predictions in regions of strain concentration: a smaller element size will generally give a higher maximum strain although at very small element sizes, further dimension changes cause little effect. Hence, strain predictions were obtained using a mesh that had been refined in the region of maximum strain in the adhesive (see figure 10). The size of elements in

the refined mesh was reduced until a stable maximum strain value had been achieved. This also gave a situation where the contour of maximum strain at an extension of 0.2 mm was greater than the size of the elements in the region of maximum strain. In all analyses, the steel adherends were assumed to be linear elastic. With both meshes, the boundary conditions were set up such that the nodes along the end of one adherend were completely constrained, while a displacement was applied to the end nodes of the other adherend (displacement control).

4.2 QUASI-STATIC ANALYSIS

The initial FE analyses were carried out under quasi-static conditions, i.e. assuming that the properties of the adhesive are independent of strain rate and that this rate is sufficiently low that inertial forces are negligible. Solutions were obtained using the von Mises, linear Drucker-Prager and exponent Drucker-Prager models to describe the behaviour of the adhesive. For these quasi-static analyses, hardening data used was measured at a strain rate of 2.65 s^{-1} (curve shown in figure 4). Results of force against extension obtained using each model are shown in figure 11. The extension is obtained from the separation between two nodes on the adherends with an initial gauge length of 25 mm. These two nodes mark the contact positions of the extensometer used in the experimental testing of lapjoints.

From figure 11 it can be seen that the von Mises analysis gives the lowest predicted force values of the three models. This is because the stress state in the adhesive is predominantly shear whilst tensile data has been used to determine the hardening function. In situations such as this, a hydrostatic stress sensitive yield criterion is needed to obtain more accurate predictions of behaviour in shear. Although the Drucker-Prager models have different dependencies of yielding on the hydrostatic stress component, these differences are not significant here because the stress state in the adhesive is predominantly shear. However, differences would be expected in the stress and strain levels predicted in regions of the joint where there is a significant hydrostatic stress component i.e. in regions of strain concentration at the ends of the adhesive layer.

4.3 DYNAMIC ANALYSIS

4.3.1 Explicit versus Implicit Analysis

A dynamic analysis takes into account the rate-dependent behaviour of adhesive properties. In ABAQUS, dynamic analyses can be carried out using either the standard (implicit) solver or the explicit solver. Both methods have advantages and disadvantages. The advantage of using the standard solver is that the initial time increment size can be chosen manually. ABAQUS then uses an automatic time incrementation scheme to adjust the increment size as necessary to obtain solutions. This means that the computer processing times are significantly shorter than when using the explicit solver, especially at the lower loading rates. With the explicit solver, the time step is determined by the time for a stress wave to cross the smallest element dimension. The result is that processing times can be excessive, especially when a refined mesh is being used, or when the analysis is at a low loading rate. The processing time can be reduced by mass scaling i.e. using artificially high values of material density, but care must be taken to ensure that inertial forces still remain insignificant.

The main advantage of the explicit code is that solutions can be obtained at larger extensions than with the standard dynamic analysis. This is illustrated in figure 12 which compares standard dynamic analyses and standard quasi-static analyses for both linear and exponent Drucker-Prager models, and the explicit analysis using the linear Drucker-Prager model. A single hardening curve with a strain rate of 2.65 s^{-1} was used for each analysis. It can be seen that the standard dynamic analysis failed to converge at a smaller extension than the standard quasi-static analysis for both models. The explicit dynamic analysis obtained solutions at higher extensions than the standard dynamic analysis. Interestingly, in this example, the standard quasi-static analysis obtained the same extension as the explicit analysis.

The explicit solver is particularly useful for analysing bonded joints made with tough adhesives that sustain large extensions before failure, such as the epoxy studied here. Unfortunately the exponent

Drucker-Prager model, which most closely describes the yielding of this adhesive, has not been implemented in ABAQUS/Explicit.

The analyses mentioned above were dynamic analyses using one hardening curve, thereby assuming an average strain rate of 2.65 s^{-1} in the lapjoint adhesive layer. More accurate predictions can be obtained by taking into account rate-dependent plasticity, and these analyses are considered in the following section.

4.3.2 Analysis with Rate-Dependent Adhesive Properties

Rate-dependent plasticity is implemented in ABAQUS by inputting data for the strain hardening function over a range of strain rates. These data are obtained from tensile tests carried out over a wide range of strain rates as discussed in section 3.3.5. The maximum strain rate obtained experimentally was 41 s^{-1} which corresponds to the mean strain rate in a lapjoint specimen at a loading speed of 10 mm/s. In order to predict joint performance at speeds of up to 1 m/s, it is necessary to extend the strain rate range for these data by a factor of approximately 100. The acquisition of hardening curves to enable predictions at these higher speeds has been described in section 3.3.5 and results are shown in figure 7.

As discussed in an earlier report (2), the exponent Drucker-Prager model is the most suitable material model for predicting the behaviour of the epoxy adhesive, so an analysis using rate-dependent plasticity was initially run using this model in ABAQUS/Standard. This analysis had convergence problems very early on, and failed to converge at an extension of less than 0.05 mm. These problems indicated that an explicit analysis would be needed to achieve predictions using rate-dependent plasticity at a reasonable extension. As the exponent Drucker-Prager model has not been incorporated into ABAQUS/Explicit V5.8, the linear Drucker-Prager model was used to obtain force/extension curves using rate-dependent plasticity. The predicted force/extension curves for lapjoint loading speeds of 1 mm/s, 10 mm/s and 100 mm/s are shown in figure 13. For each prediction, four hardening curves were used, one with a strain rate approximately the same as the

average strain rate in the lapjoint, one higher strain rate curve, one lower strain rate curve, and an even lower strain rate curve which is designated as the zero rate curve.

In order to predict rupture of the joint and evaluate the failure criterion developed in earlier work (1), accurate values for the maximum strain in the adhesive are needed. The most accurate predictions of strain that can be obtained using available models are considered to be those derived using the exponent Drucker-Prager model. Since convergence problems arise when using this model with rate-dependent hardening curves and ABAQUS/standard, strain predictions have been obtained using a single strain hardening curve which gives a comparable force/extension curve to that which would be obtained from an analysis using four hardening curves. It is apparent from figures 12 and 13 that the force/extension curves predicted using the linear Drucker-Prager model with a single hardening curve at 2.65 s^{-1} match closely with the rate-dependent prediction at a loading speed of 1 mm/s. The explicit solver was used for these analyses as there were also convergence problems for the linear Drucker-Prager model using rate-dependent data in ABAQUS/standard. To improve the correlation between the predictions, new hardening curves were generated at various strain rates. It was found that at a loading speed of 1 mm/s, the explicit rate-dependent predictions compared well with a single rate prediction with a strain rate of 3 s^{-1} (see figure 14).

It is assumed that a factor of 10 increase in loading rate will give a factor of 10 increase in the mean strain rate in the adhesive region of the lapjoint. This assumption is supported by the results shown in figure 15 which compare force/extension predictions from an explicit analysis with four hardening curves and a loading rate of 0.1 mm/s with the single hardening curve prediction from a standard analysis at a strain rate of 0.3 s^{-1} . It is now possible to run implicit (standard) exponent Drucker-Prager analyses using these mean strain rates to obtain a suite of force/extension predictions over a range of lapjoint loading speeds. These are shown in figure 16. The predicted curves are all evenly spaced, although it is noted that the predictions at lower load rates had convergence problems at lower extensions.

4.4 STRAIN CALCULATIONS

The magnitude of the peak strain predicted in the adhesive region is dependent on the material model used. Analyses run with the exponent Drucker-Prager model give higher strain predictions than those run with the linear Drucker-Prager model. Ideally we want exponent Drucker-Prager predictions using rate-dependent data, although we are not able to obtain these predictions directly. An attempt has therefore been made to obtain best estimates of strain by inference using the results of different strain predictions. The maximum strain in the adhesive (using the refined mesh) can be obtained at any loading rate and extension with the following analyses:

- explicit linear Drucker-Prager analysis with 4 hardening curves
- explicit linear Drucker-Prager analysis with 1 hardening curve
- implicit exponent Drucker-Prager analysis with 1 hardening curve

The maximum strain value in the adhesive predicted for an exponent Drucker-Prager analysis using rate-dependent data can be inferred from a similar analysis using a single rate hardening curve. This can be achieved by comparing the maximum strain values predicted for a linear Drucker-Prager analysis using rate-dependent data and a similar analysis using a single hardening curve. The relationship between predictions using four hardening curves and those using a single hardening curve is assumed to be the same for both linear Drucker-Prager and exponent Drucker-Prager models. This calculation would need to be carried out at each lapjoint loading speed as, from studying the predictions, it appears that this relationship is also rate-dependent.

For a lapjoint loading speed of 0.1 mm/s at an extension of 0.18 mm, the calculations yield the following results:

maximum principle logarithmic strain (explicit; linear D-P; 4 rates) = 0.449

maximum principle logarithmic strain (explicit; linear; 1 rate) = 0.67

maximum principle logarithmic strain (implicit; exponent; 1 rate) = 0.932

therefore:-

max principle logarithmic strain (implicit; exponent; 4 rates) = $0.932 \cdot (0.449/0.67) = 0.625$

In a later section, this method will be used to obtain predictions of the peak strain in the adhesive layer of the lapjoint. These strains will then be used to investigate the validity of the failure criterion.

5 EXPERIMENTAL TESTS ON THE LAP-JOINT SPECIMENS

Tensile tests on lapjoint specimens have been carried out under controlled displacement rate conditions in a servohydraulic test machine. Loading speeds within the range 0.1 mm/s to 100 mm/s were used. The extension of the joint was measured using extensometers (with gauge length of 25 mm) attached to the wide faces of the lapjoint adherends. Two extensometers were used to improve measurement accuracy. A series of force vs lap shear strength curves were obtained at the different loading speeds. The curves are presented in figure 17 and are typical of results obtained from several sets of test specimens. The extension at failure varies between 0.25 mm and 0.45 mm implying a mean shear strain in the adhesive at failure of between 50-90%. After reaching a maximum load, the force drops off gradually before the lapjoint fails. In these tests, the acceleration of the actuator to reach the set speed is achieved within a displacement of 0.1 mm. The remainder of the test is then carried out under constant speed.

6 EVALUATION OF A FAILURE CRITERION

A criterion for ductile failure of the adhesive under short-term monotonic loading has been proposed in earlier work (1) based on the development of a critical level of strain in the adhesive. Previous studies of failure in bulk specimens under tension and butt-joint specimens under tension and shear indicated that a component of hydrostatic (volumetric) strain must be present in the adhesive to initiate failure. The critical level of this strain is however dependent upon the level of any shear strain component. A criterion could then be defined by plotting the results of the above failure tests on axes of the hydrostatic strain component against the shear strain component. These axes are

conveniently expressed in terms of the invariants I_1 (the volumetric strain) and $I_{2D}^{1/2}$ (the effective shear strain). Values for the magnitude of these invariants in each test at failure are derived from components of the true principal strain ϵ_{1f} , ϵ_{2f} and ϵ_{3f} at failure using the equations

$$I_{1f} = \epsilon_{1f} + \epsilon_{2f} + \epsilon_{3f} \quad (17)$$

$$I_{2Df}^{1/2} = \left\{ \frac{1}{6} \left[(\epsilon_{1f} - \epsilon_{2f})^2 + (\epsilon_{2f} - \epsilon_{3f})^2 + (\epsilon_{3f} - \epsilon_{1f})^2 \right] \right\}^{1/2} \quad (18)$$

The results of a selection of tensile tests on bulk specimens of the adhesive are shown in figure 18. These were selected from a larger number of tests carried out on specimens that had been cut from plates cast from different cartridges. The results illustrate the wide range of failure strains, 0.02 to 0.08, that have been measured in these tests. It was observed that polishing the machined edges of specimens in order to reduce any influence of surface flaws had no effect on the measured failure strain. Furthermore, specimens tested soon after machining gave similar failure strains to other specimens from the same sheet that were stored for several weeks in a dessicator prior to testing. This implies that small changes in the concentration of absorbed water from the atmosphere are not responsible for the wide variation in the strain at failure. Some typical results of tensile tests on butt-joint specimens of the epoxy adhesive are shown in figure 19. In contrast to the results on bulk specimens, failure strains obtained with butt-joint specimens showed very little variation and were consistently close to a value of 0.07.

From estimates of the failure strains in figures 18 and 19, the magnitudes of the strain invariants at failure, I_{1bf} and $I_{2Dbf}^{1/2}$ for the butt-joint specimens and I_{1uf} and $I_{2Duf}^{1/2}$ for the uniaxial tension specimens, can be calculated using equations (17) and (18). For this purpose we note that, under uniaxial tension, $\epsilon_{2uf} = \epsilon_{3uf} = -\nu_f \epsilon_{1uf}$ and under butt-tension $\epsilon_{2bf} = \epsilon_{3bf} = 0$ for applied stresses along the 1-axis. Values for the strain components in equations (17) and (18) at failure are shown in table 4.

**Table 4 – Values obtained for strain components at failure in
tensile tests on bulk and butt-joint specimens of the
epoxy adhesive**

ϵ_{1uf}	ϵ_{1bf}	V_f	I_{1uf}	$I_{2Duf}^{1/2}$	I_{1bf}	$I_{2Dbf}^{1/2}$
0.02-0.08	0.075	0.29	0.01-0.034	0.015-0.06	0.075	0.045

Failure strains are plotted on axes of I_1 against $I_{2D}^{1/2}$ in figure 20. The failure criterion proposed in earlier work (1) must approach the $I_{2D}^{1/2}$ axis asymptotically. This is to satisfy the condition that failure will only occur under pure shear at very large strain. If this criterion is to describe the data in figure 20, then it is only the higher strain values for the bulk specimen data that are consistent with the butt-joint failure data. The observation that failure can occur in bulk specimens at somewhat smaller strains may be relevant to the interpretation of tests on the lap-joint specimens that is discussed in the next section.

7 COMPARISON OF MEASURED AND PREDICTED JOINT PERFORMANCE

7.1 FORCE/EXTENSION BEHAVIOUR

Predicted and measured force/extension curves obtained for the lap-joint specimen at deformation speeds of between 0.1 mm/s and 100 mm/s are compared in figure 21. At small extensions, where the deformation behaviour of the adhesive is linear, the predicted force/extension curves agree reasonably well. However at larger extensions, the correlation deteriorates. The measured curves become non-linear at lower stresses than predicted for the onset of non-linear behaviour. The predicted maximum loads are consistently higher than measured loads. Also, once the predicted maximum load has been reached, the force stays at this level until the analysis ends in contrast to the decrease in load observed in the experimental tests. Possible sources of error in the finite element analysis have been investigated. Figure 22 compares predictions made with elastic-plastic steel adherends at a single loading speed of 10 mm/s. The plastic hardening data assumed for the steel

were typical values but may not be accurately representative of the grade of steel used in the lap-joint tests. Whilst plastic deformation of the steel is observed to lower the predicted force, the shape of the force/extension curve is quite different from that measured. Furthermore, measured force/extension curves obtained on a set of lap-joint specimens with hardened steel adherends showed no significant difference to the curves illustrated here. It seems therefore that, whilst plasticity in the adherends should, in general, be included in an analysis, it does not explain the discrepancy between measured and predicted results obtained here.

Also shown in figure 22 is a predicted curve using a generalised plane strain analysis with elastic adherends. It can be seen that this analysis has no effect on force/extension curve predictions.

The observed difference between measured and predicted lap-joint deformation is consistent with that seen in a previous report (3) on the Ciba adhesive LMD1142. In the previous work it was thought that these differences may have been due to differences in properties between the adhesive in the lap-joint and the bulk specimens used to obtain hardening data. For the work reported here, an effort had been made to investigate possible differences between bulk and joint adhesive properties through comparisons of results obtained on bulk specimens prepared with different cure temperatures, cure times and thicknesses. The conclusions from that investigation, discussed in section 3.1, indicate that the tensile properties are insensitive to cure conditions and specimen thickness.

7.2 EVALUATION OF THE FAILURE CRITERION

An alternative explanation considered in the previous report, is that the adhesive is failing locally at the extension where the measured and predicted curves depart. This will lead to a reduction in the amount of adhesive that is able to sustain load. Hence there will be an increase in the stress level in the remainder of the adhesive. The adhesive will then reach the flow stress appropriate to each strain rate at a lower force than predicted for the undamaged bond. This explanation was initially considered unlikely because the maximum strain level in the adhesive at the extension of the joint where the measured and predicted curves depart (approx 0.05 mm) is well below the strain at

which failure would be expected from tensile tests on bulk and butt-joint specimens. However, results on bulk specimens of the adhesive studied here and shown in figure 18 reveal that, under some circumstances, failure in the adhesive can occur at uniaxial tensile strains as low as 0.02. Strain distributions in the adhesive were therefore calculated at an extension of 0.05 mm. As explained in section 4.3.2, solutions using a dynamic analysis with rate-dependent hardening data cannot be obtained beyond very small extensions with the exponent Drucker-Prager model. Figure 23 shows distributions of the maximum principal strain obtained with the exponent Drucker-Prager model and a single hardening curve at a strain rate of 0.3 s^{-1} . It can be seen that the peak in strain occurs in the adhesive at the end of the curved surface of the adherend. However, there is another, lower strain concentration on the curved surface of the fillet. The maximum strain here is about 0.02 which is similar to the lower bound of failure strains in bulk specimens under tension. If failure of the adhesive were to initiate here and propagate normal to the fillet surface, then the volume of the adhesive bearing load and the load bearing capacity of the joint will be reduced. To explore this situation further, the finite element mesh was modified as shown in figure 24, and a force/extension curve was predicted. The results are plotted in figure 25 using a single hardening curve at 0.3 s^{-1} , and are compared here with the curve for the original mesh and experimental data at a speed of 0.1 mm/s.

For this situation, the predicted force/extension curve is significantly closer to the measured data. It is possible that the predicted curve would be even closer if proper account could be taken in the FE analysis of rate dependent plastic deformation in the adhesive. The new model currently under development for toughened adhesives should also give a better description of plastic deformation in the adhesive.

It is also likely that further progressive rupture of the adhesive is taking place as the extension of the joint is increased. The distribution of the maximum principal strain in the adhesive obtained at an extension of 0.1 mm using the above analysis for the partly ruptured fillet is shown in figure 26. This reveals that the region of strain concentration has moved to the junction of the crack in the fillet and the adherend. The magnitude of calculated strains in this region will be dependent on the shape of the surface of the adhesive and the local element size. The peak value of about 0.1 shown in the figure is consistent with the rupture strain of butt-joint specimens in tension (figure 19). This implies

that joint rupture will continue in a progressive process and will consequently explain the fall in load observed in experimental curves at extensions above around 0.15 mm.

8 CONCLUSIONS AND FURTHER WORK

Two materials models have been used with finite element analyses to predict the deformation behaviour of lap-joint specimens bonded with a modern toughened epoxy adhesive. Earlier work on butt-joint specimens loaded in tension indicated that the exponent Drucker-Prager model would give more accurate predictions than the linear Drucker-Prager.

Materials property data required by these models can be determined from a combination of tensile and shear tests on bulk specimens. Rate-dependent plasticity can be modelled if tensile data are generated over a range of testing speeds. The tensile properties of bulk specimens of the toughened epoxy studied here are not sensitive to the specimen thickness in the range 1 to 3 mm nor to changes in the curing time within the range used for the preparation of bulk and joint specimens.

It was only possible to obtain solutions with these models and the ABAQUS standard solver out to moderate extensions of the joint specimen if rate-dependent plasticity was ignored. Solutions with rate-dependent plasticity required use of the explicit solver.

Predicted force/extension curves for the lap-joint specimen lie consistently at higher force levels than measured curves over a range of loading speeds. The reason for this is not clear but is believed to arise through progressive failure in local regions of the adhesive starting in the fillet. This explanation is only plausible if rupture in the fillet can occur at low strains (~ 0.02). This is well below the strain level at which failure occurs in butt-joint specimens loaded in tension but has been observed in some tensile tests on bulk specimens. Bulk specimens loaded in tension have been observed to fail over a wide range of tensile strain.

When part of the fillet region is removed from the finite element mesh, force/extension predictions lie significantly closer to measured values. Further progressive failure of the adhesive is then implied by a comparison of predicted and measured curves.

Further work is needed to explain the wide variation of failure strains observed in tensile tests on bulk specimens. Any correlation between failure in bulk and joint specimens of an adhesive also needs to be clarified.

Predictions of force/extension curves and strain distributions will be made using the new materials model currently under development. This model takes account of the important contribution from cavitation in the adhesive to the toughness and deformation behaviour of the adhesive. These predictions will be compared with the predictions and measurements reported here.

9 ACKNOWLEDGEMENTS

The important contributions of Mr A Pearce and Ms E Arrantz to the experimental testing of bulk and joint specimens is gratefully acknowledged.

The work was funded by the Department of Trade and Industry as part of The Performance of Adhesive Joints programme.

REFERENCES

1. G Dean and L Crocker. A proposed failure criterion for tough adhesives. NPL Report CMMT(A)158, February 1999.
2. G Dean, B Read and B Duncan. An evaluation of yield criteria for adhesives for finite element analysis. NPL Report CMMT(A)117, January 1999.
3. G Dean, G Lord and B Duncan. Comparison of the measured and predicted performance of adhesive joints under impact. NPL Report CMMT(A)198, October 1999.
4. G Dean, B Duncan, R Adams, R Thomas and L Vaughn. Comparison of bulk and joint specimen tests for determining the shear properties of adhesives. NPL Report CMMT(B)51, April 1996.
5. B Duncan. Methods for measuring strains at high rates. NPL Report CMMT(A)133, November 1998.

FIGURE CAPTIONS

- Figure 1 Tensile stress/strain curves for the epoxy adhesive for specimens of different thickness and cure rate.
- Figure 2 Stress/strain curves for the epoxy adhesive in tension and shear measured at the same effective plastic strain rate of 0.002 s^{-1} .
- Figure 3 Plots of effective stress $\bar{\sigma}$ (see equation (12)) against effective plastic strain $\bar{\epsilon}_p$ (see equation (9)) derived from the data in figure 2.
- Figure 4 Tensile stress/strain curves for the epoxy adhesive measured at different strain rates.
- Figure 5 Rate-dependent hardening curves for the epoxy adhesive obtained from the data in figure 4. The continuous curves are fits to the data using equation (15).
- Figure 6 Plots showing the linear dependence of the parameters σ_f and σ_o upon $\log \epsilon_p$ according to equation (16).
- Figure 7 Rate-dependent hardening curves for the epoxy adhesive showing comparisons between experimental data and behaviour modelled using equations (15) and (16) and the values for the parameters in table 3.
- Figure 8 Schematic diagram of the lap-joint test specimen.
- Figure 9 The mesh used for initial FE analysis of the lap-joint specimen.
- Figure 10 The refined mesh used to obtain predictions of the peak strain in the adhesive.
- Figure 11 Comparison of force vs extension predictions of the lap-joint specimen. All predictions obtained from quasi-static analyses using a hardening curve at a strain rate of 2.65 s^{-1} .
- Figure 12 Comparison of force/extension predictions obtained using both static and dynamic analysis. A single hardening curve obtained at a strain rate of 2.65 s^{-1} was used.
- Figure 13 Force/extension predictions for explicit analyses with rate-dependent plasticity.
- Figure 14 Comparison of the 1 mm/s force/extension prediction from an explicit analysis with rate-dependent plasticity with the prediction obtained using a single strain rate hardening curve (3 s^{-1}).
- Figure 15 Comparison of the 0.1 mm/s force/extension prediction from an explicit analysis with rate-dependent plasticity with the prediction obtained using a single strain rate hardening curve (0.3 s^{-1}).

- Figure 16 Force/extension predictions for 4 loading rates (0.1 mm/s – 100 mm/s). The exponent Drucker-Prager model was used with the relevant single strain rate hardening curve and a refined mesh.
- Figure 17 Experimental force/extension curves obtained for lap-joint specimens tested at speeds between 0.1 mm/s and 100 mm/s.
- Figure 18 Selected tensile stress/strain curves for bulk specimens of the epoxy showing the wide range of measured strains at failure.
- Figure 19 Stress/strain curves for butt-joint specimens tested in tension.
- Figure 20 Plots of strain invariants I_1 vs $I_{2D}^{1/2}$ (see equations 17 and 18) at failure from tensile tests on bulk and butt-joint specimens of the epoxy. Data are taken from table 4.
- Figure 21 Comparison of predicted force/extension curves at different loading speeds with measurements made using controlled displacement rate tests.
- Figure 22 Force/extension curves at a speed of 10 mm/s comparing the results of analyses obtained for plasticity in the steel adherends and generalised plane strain elements.
- Figure 23 Calculated distribution of the maximum principal strain in the lap-joint at 0.05 mm extension.
- Figure 24 The mesh used to obtain predictions for a lap-joint specimen after partial rupture in the fillet region.
- Figure 25 Comparison of force/extension curves for the complete and partially ruptured lap-joint with experimental data at 0.1 mm/s. Exponent Drucker-Prager model with a single hardening curve at a strain rate of 0.3 s^{-1} .
- Figure 26 Distribution of the maximum principal strain in the lap-joint at 0.1 mm extension following the onset of rupture in the fillet.

FIGURES

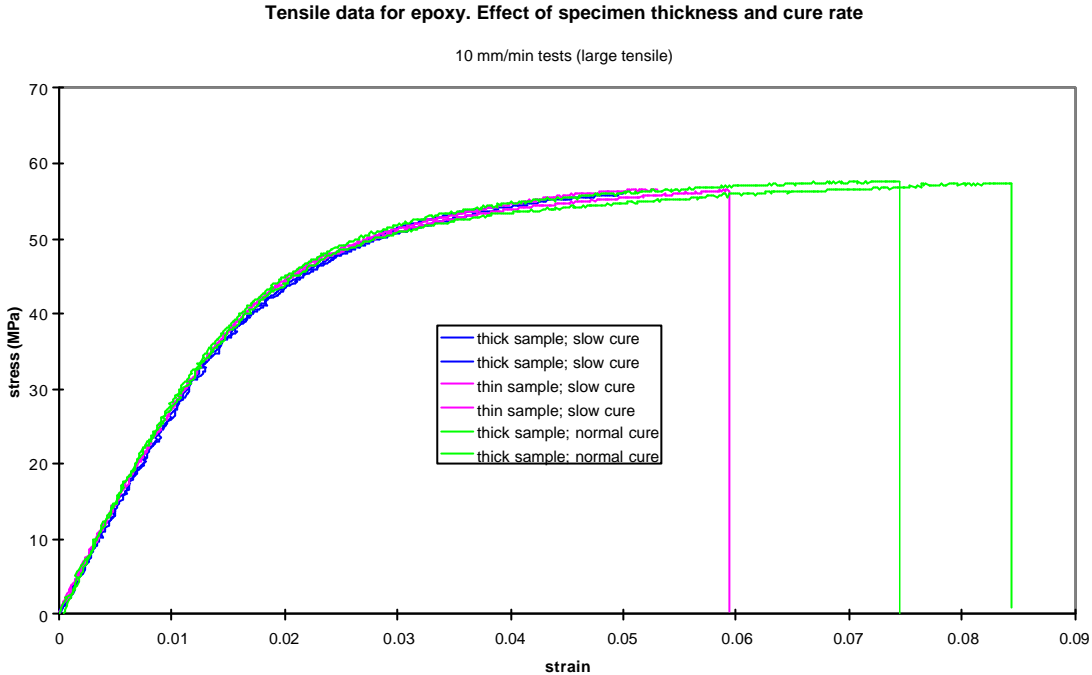


Figure 1. Tensile stress/strain curves for the epoxy adhesive for specimens of different thickness and cure rate.

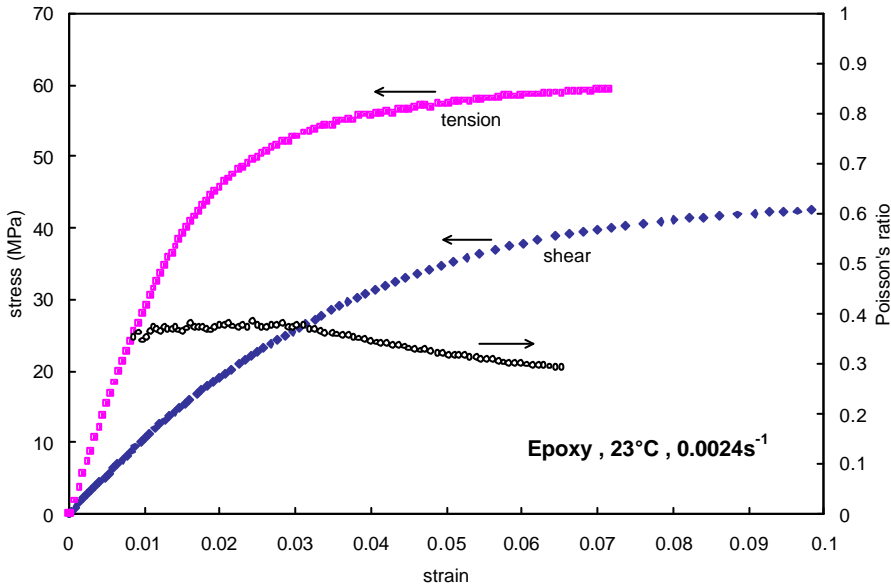


Figure 2. Stress/strain curves and Poisson's ratio for the epoxy adhesive in tension and shear measured at the same effective plastic strain rate of 0.002 s⁻¹.

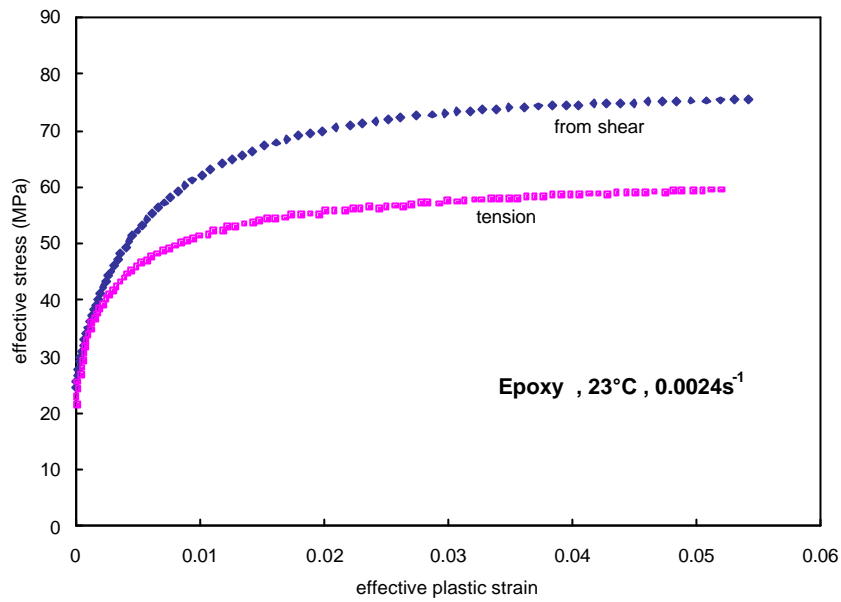


Figure 3. Plots of effective stress \bar{s} (see equation (12)) against effective plastic strain \bar{e}_p (see equation (9)) derived from the data in figure 2.

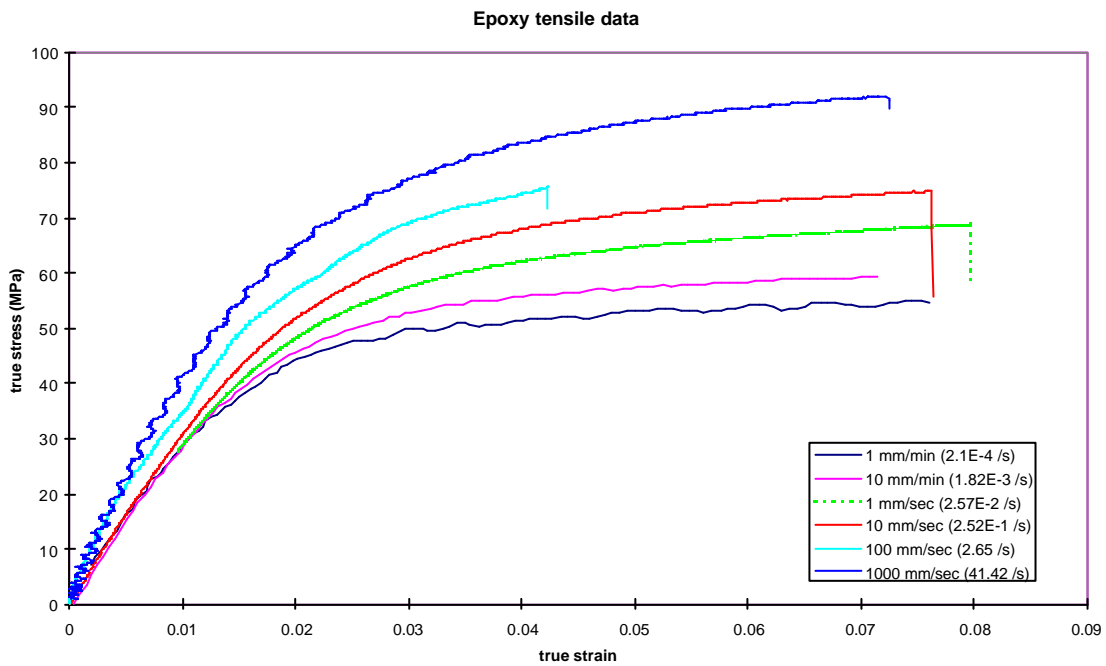


Figure 4. Tensile stress/strain curves for the epoxy adhesive measured on bulk specimens at different strain rates.

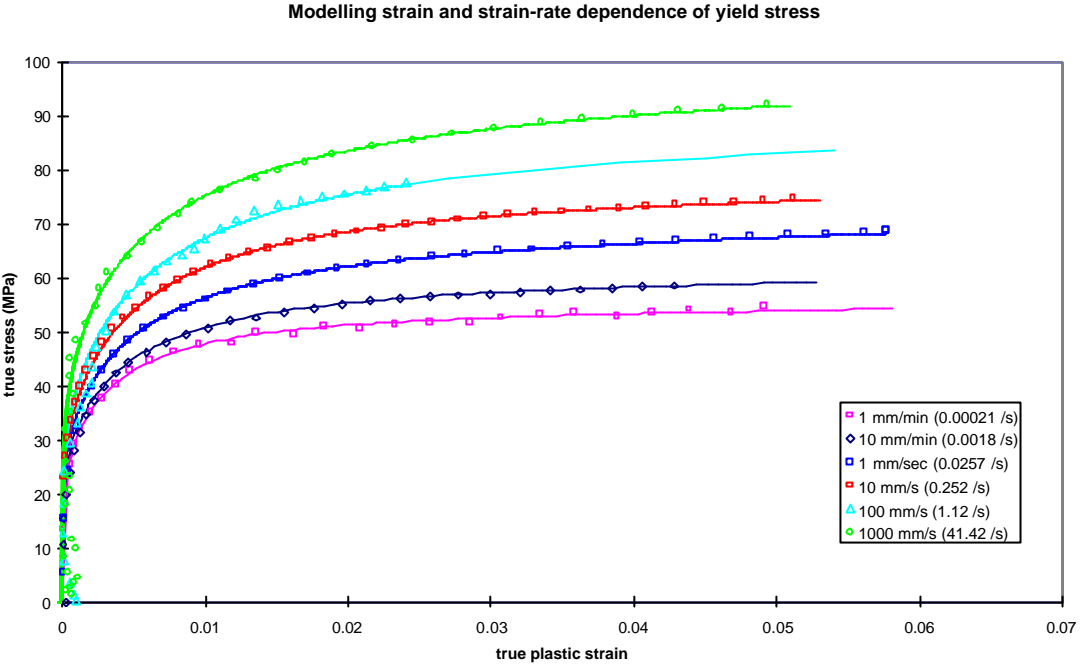


Figure 5. Rate-dependent hardening curves for the epoxy adhesive obtained from the data in figure 4. The continuous curves are fits to the data using equation (15).

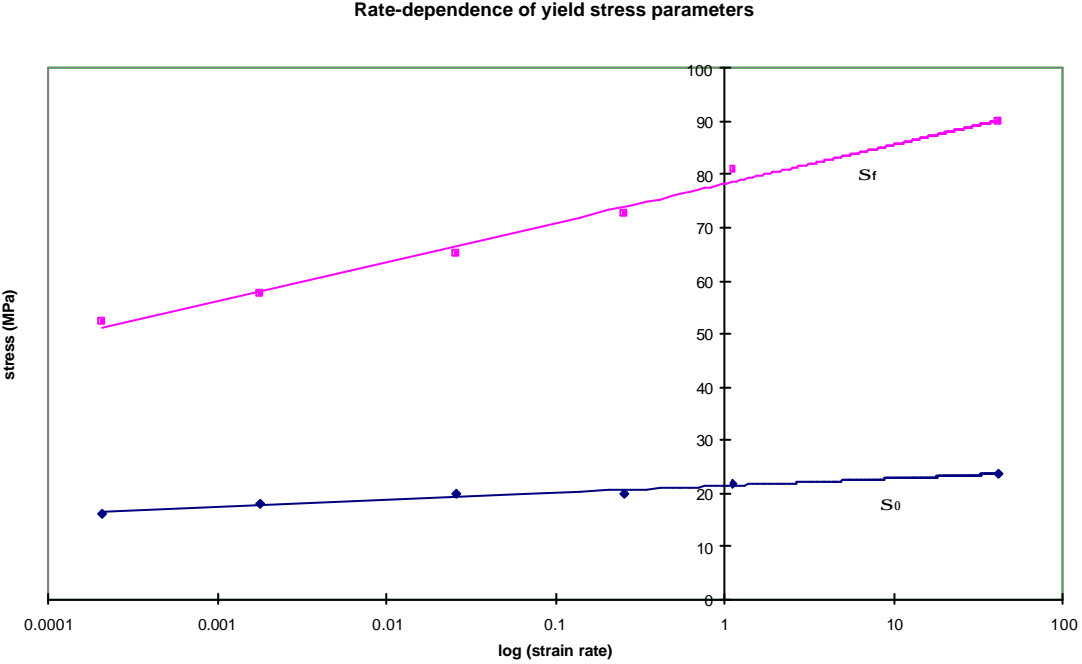


Figure 6. Plots showing the linear dependence of the parameters σ_f and σ_o upon $\log \epsilon_p$ according to equation (16).

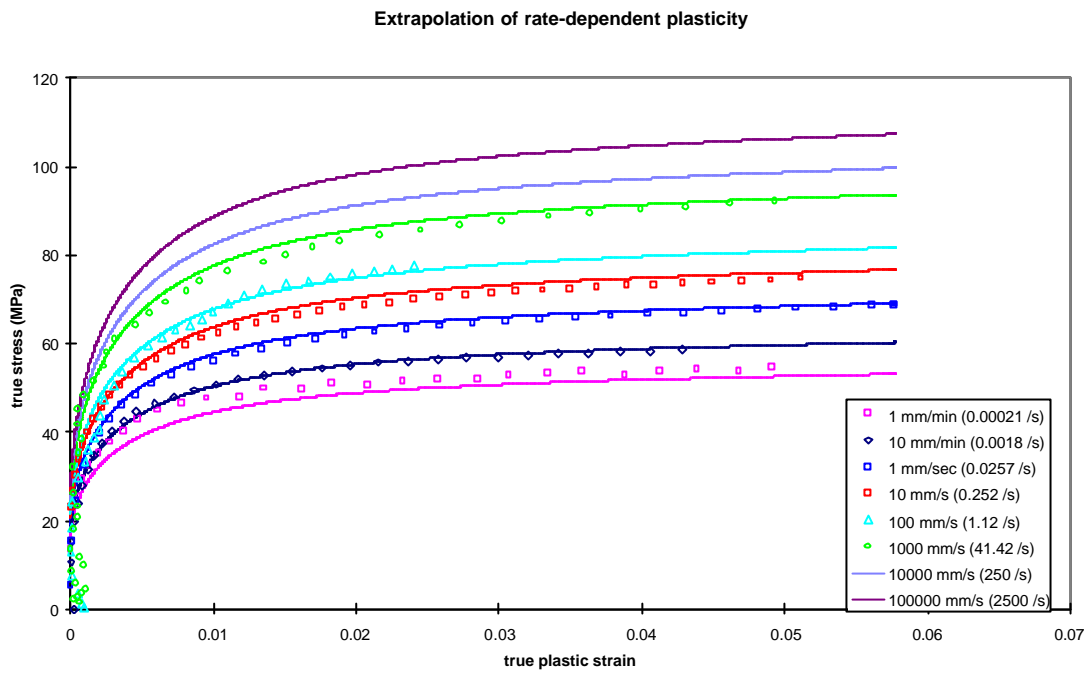


Figure 7. Rate-dependent hardening curves for the epoxy adhesive showing comparisons between experimental data and behaviour modelled using equations (15) and (16) and the values for the parameters in table 3.

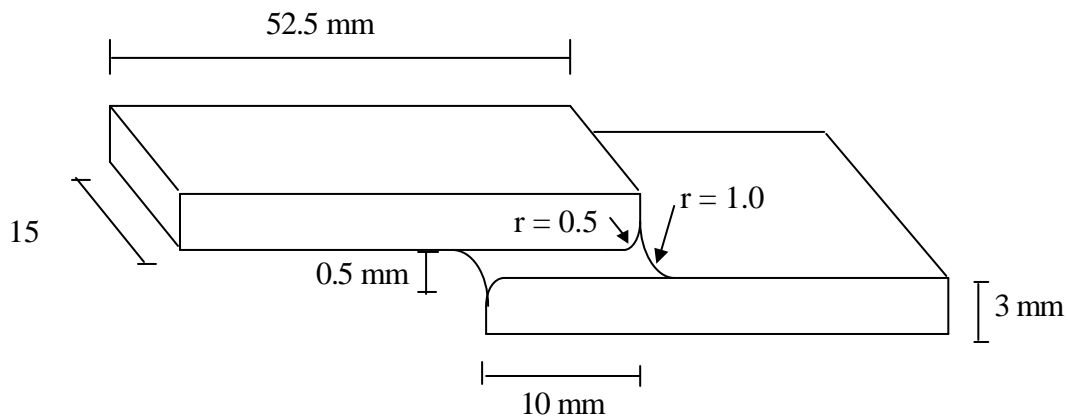


Figure 8. Schematic diagram of the lapjoint test specimen.

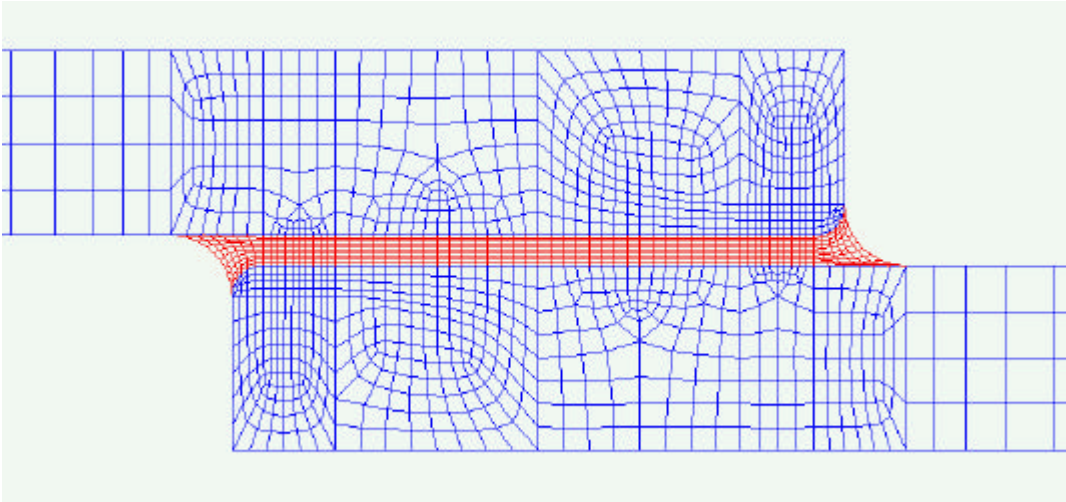


Figure 9. The mesh used for initial FE analysis of the lapjoint specimen.

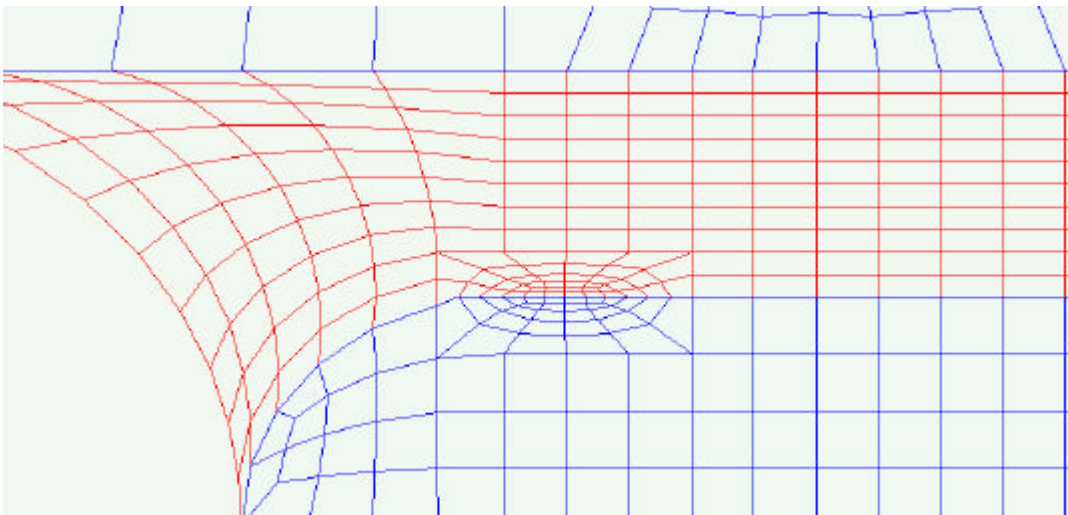


Figure 10. The refined mesh used to obtain predictions of the peak strain in the adhesive.

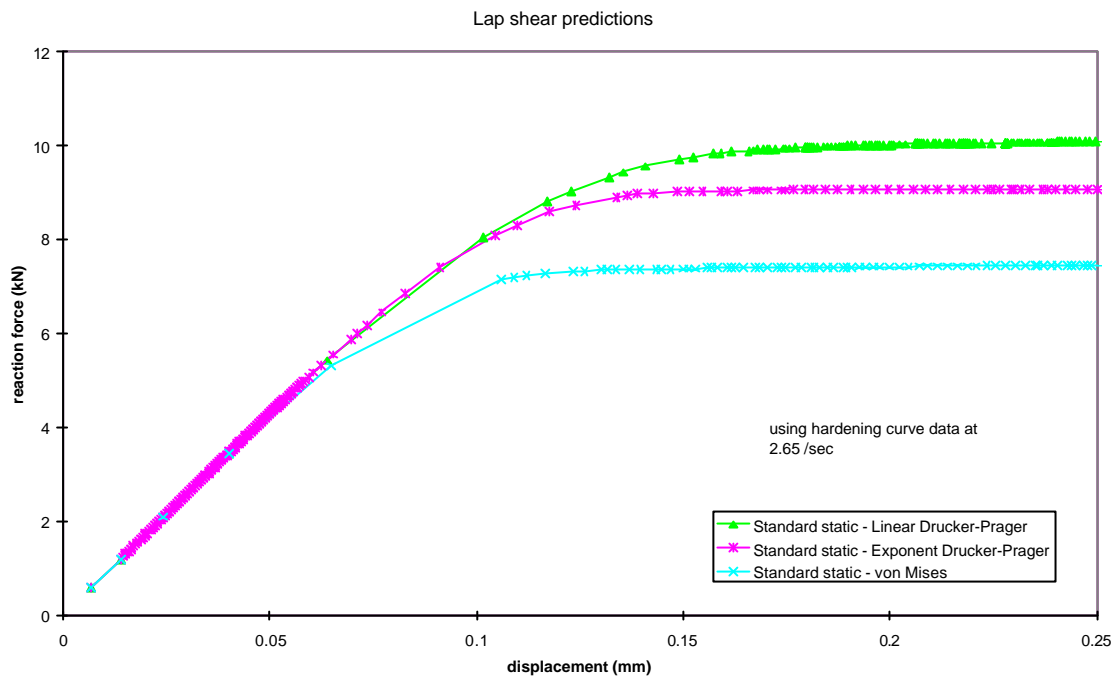


Figure 11. Comparison of force vs extension predictions of the lapjoint specimen. All predictions obtained from quasi-static analyses using a hardening curve at a strain rate of 2.65 s⁻¹.

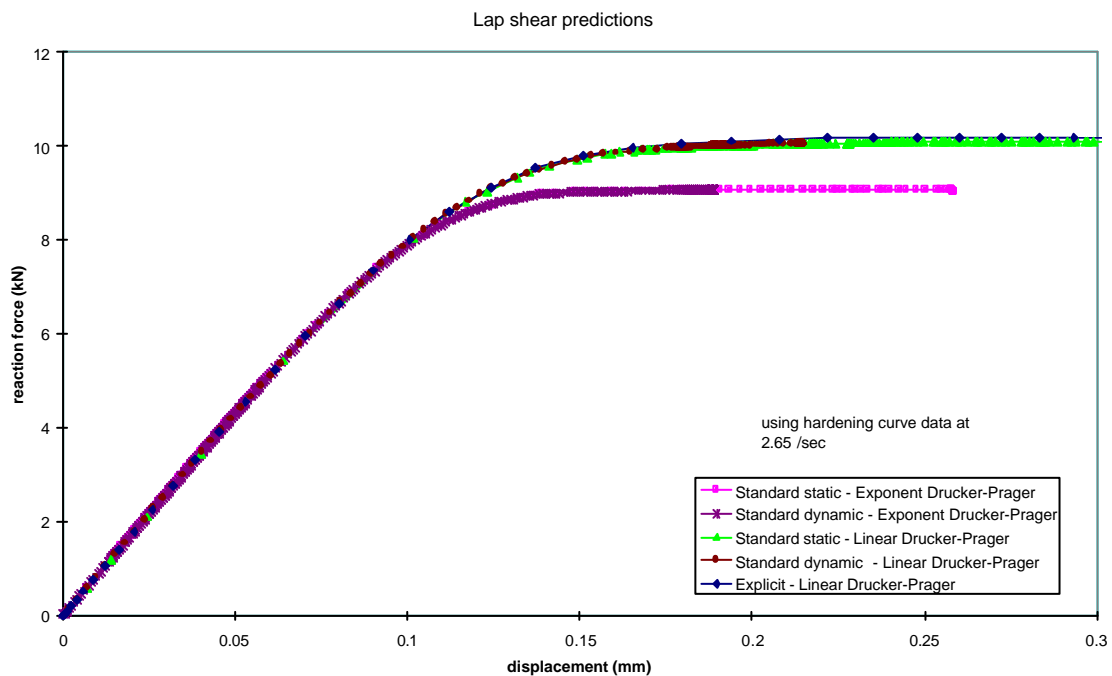


Figure 12. Comparison of force/extension predictions obtained using both static and dynamic analysis. A single hardening curve obtained at a strain rate of 2.65 s⁻¹ was used.

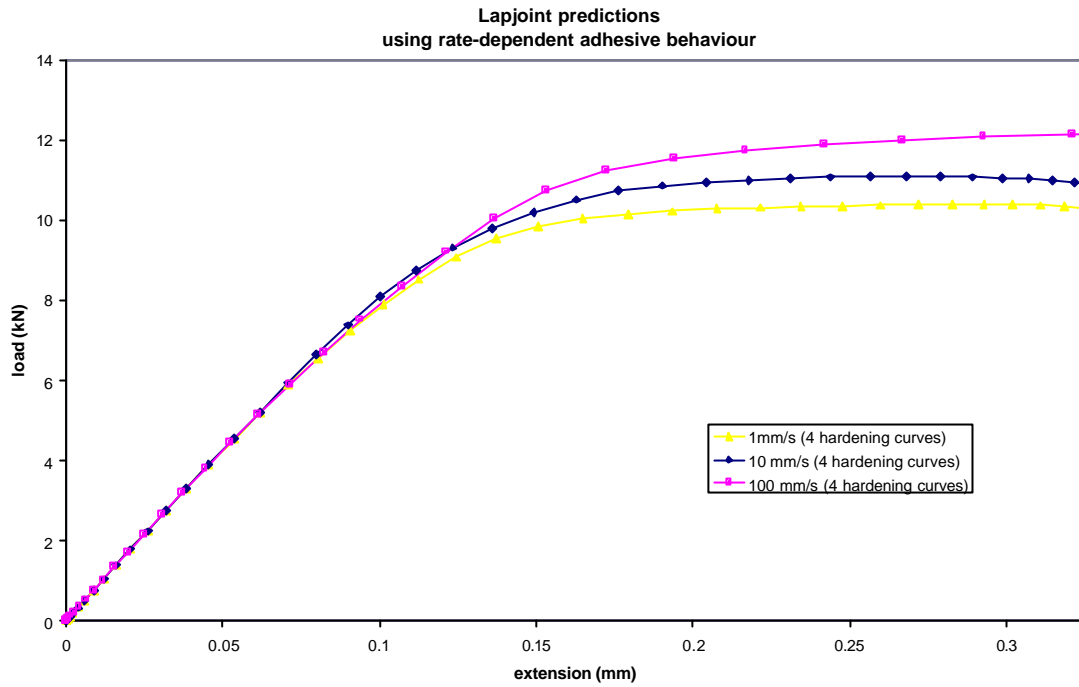


Figure 13. Force/extension predictions using the linear Drucker-Prager model with rate-dependent plasticity and the explicit solver.

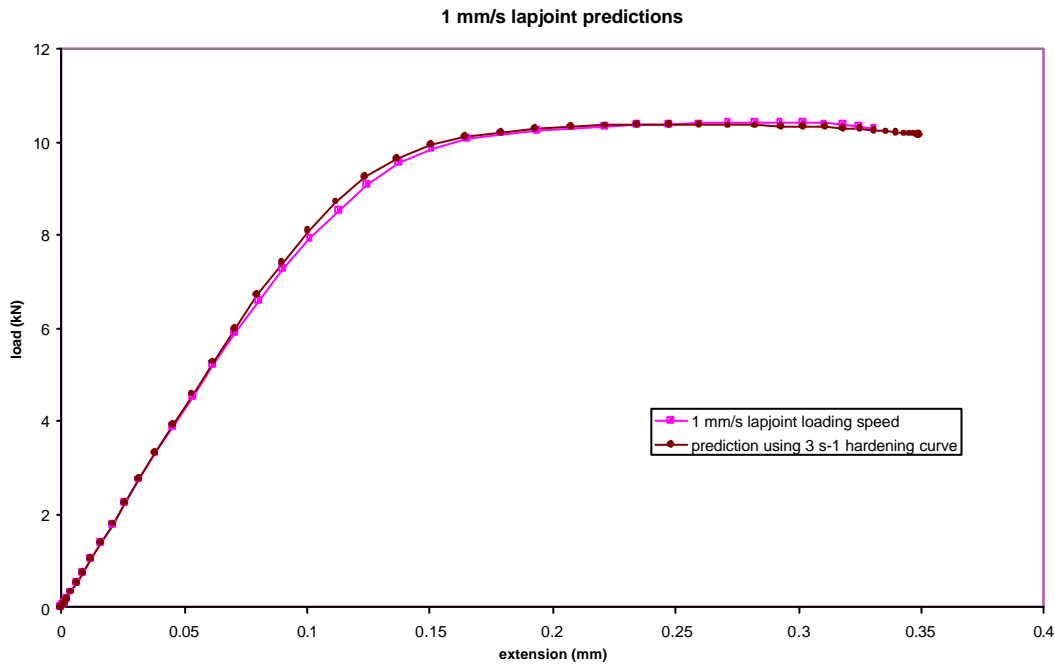


Figure 14. Comparison of the 1 mm/s force/extension prediction from an explicit analysis with rate-dependent plasticity with the prediction obtained using a single strain rate hardening curve (3 s⁻¹). Linear Drucker-Prager model.

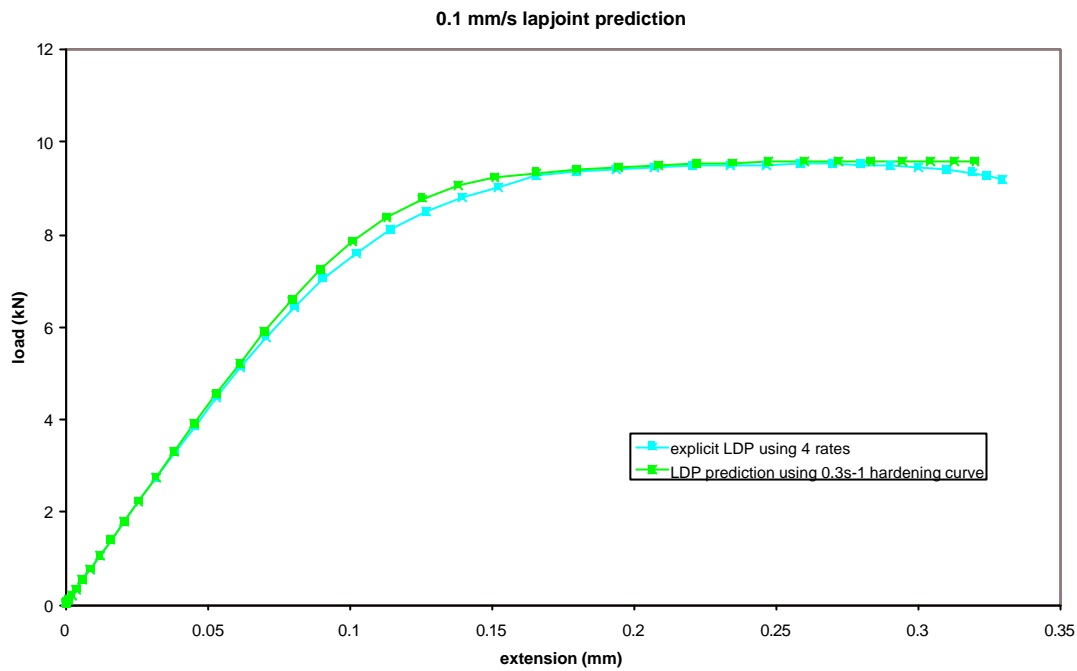


Figure 15. Comparison of the 0.1 mm/s force/extension prediction from an explicit analysis with rate-dependent plasticity with the prediction obtained using a single strain rate hardening curve (0.3 s⁻¹).

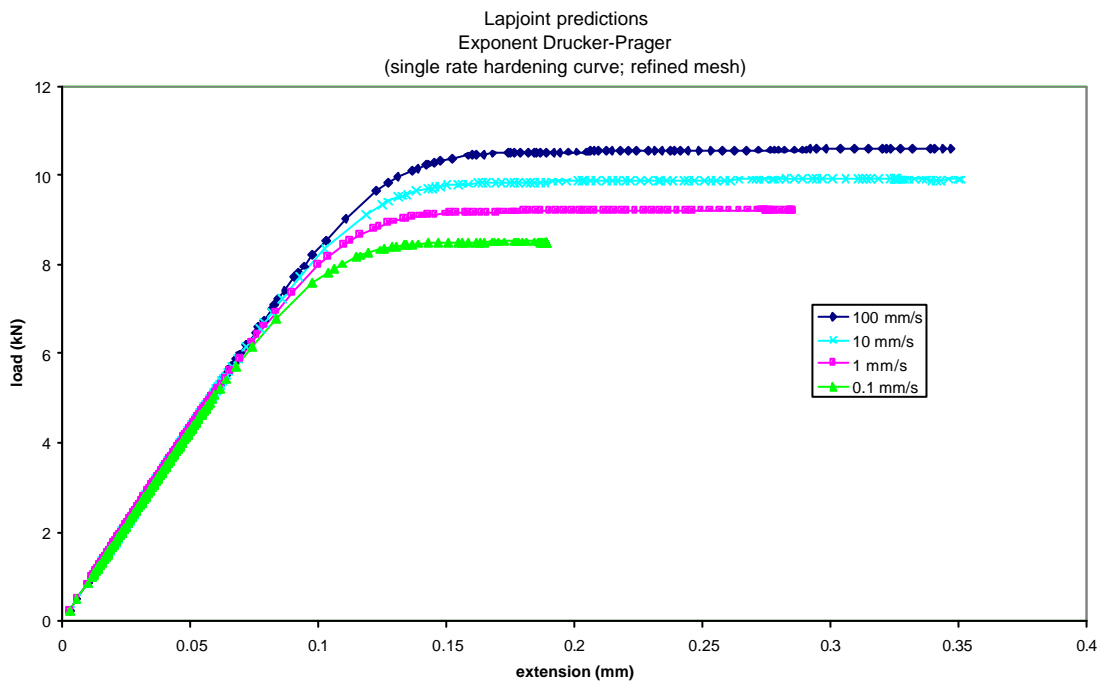


Figure 16. Force/extension predictions for 4 loading rates (0.1 mm/s – 100 mm/s). The exponent Drucker-Prager model was used with the relevant single strain rate hardening curve and a refined mesh.

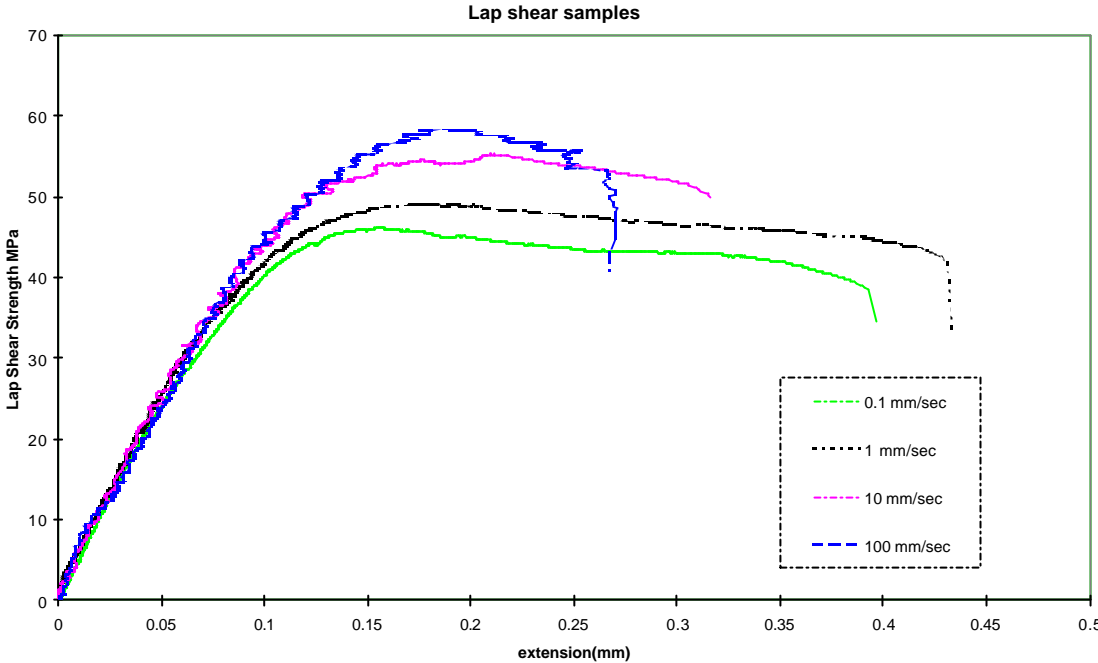


Figure 17. Experimental force/extension curves obtained for lapjoint specimens tested at speeds between 0.1 mm/s and 100 mm/s.

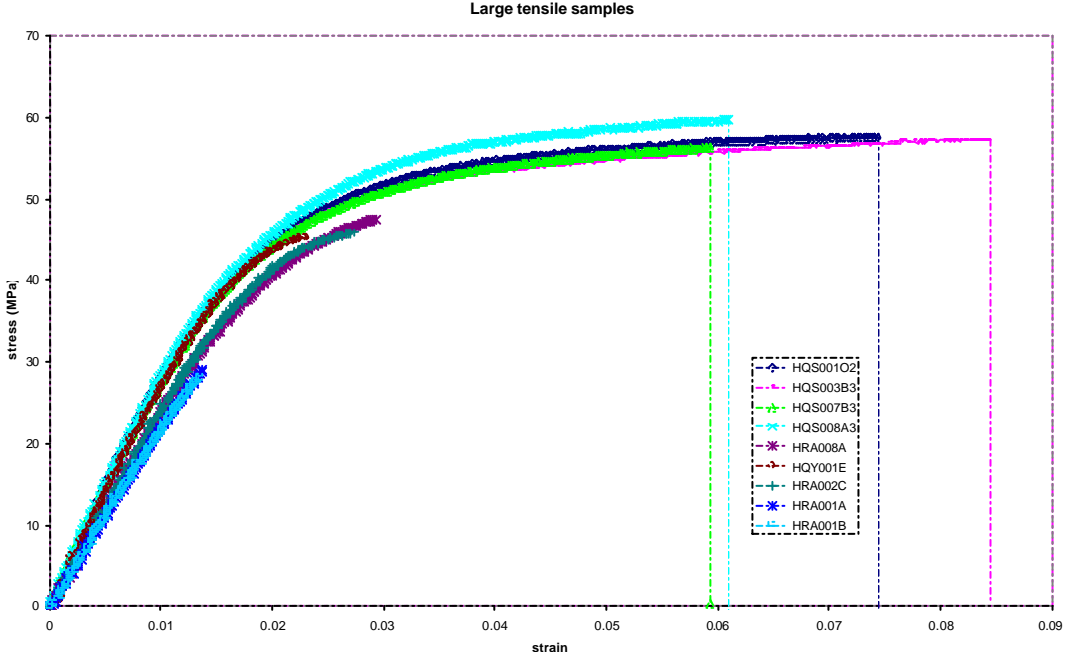


Figure 18. Selected tensile stress/strain curves for bulk specimens of the epoxy showing the wide range of measured strains at failure.

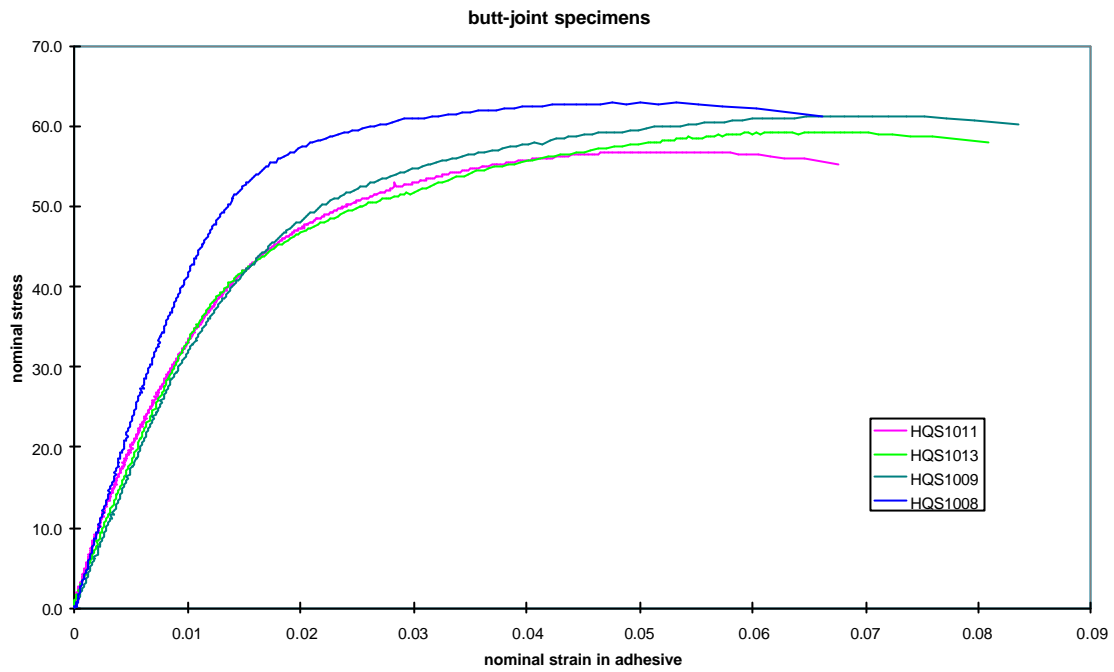


Figure 19. Stress/strain curves for butt-joint specimens tested in tension.

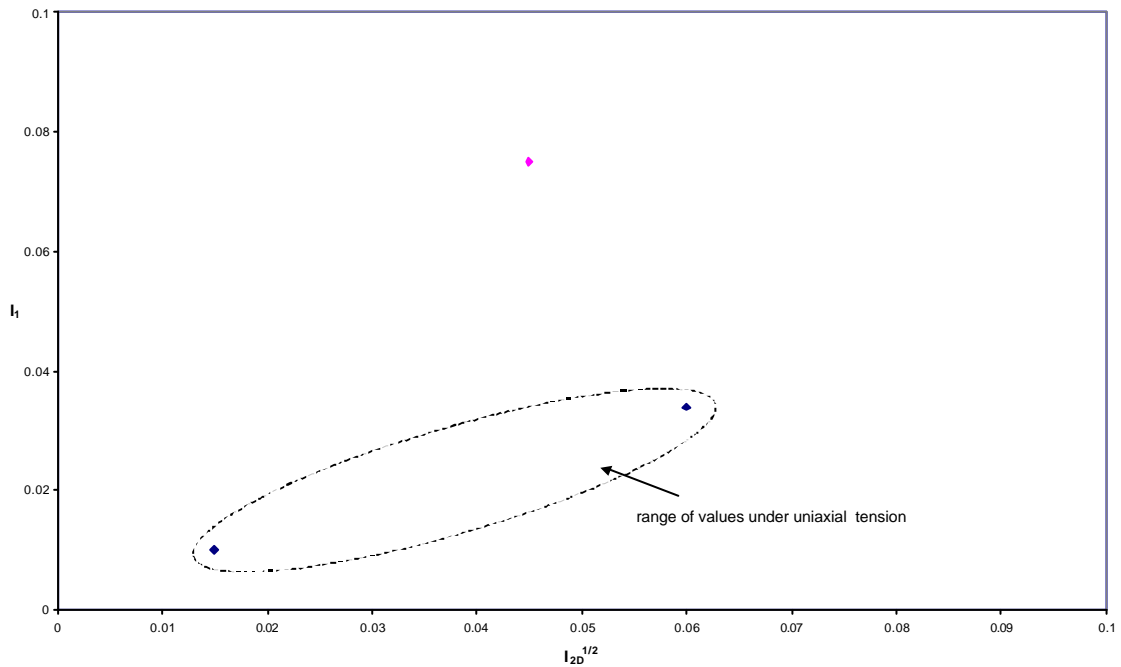


Figure 20. Plot of strain components I_1 vs $I_{2D}^{1/2}$ (see equations 17 and 18) at failure from tensile tests on bulk and butt-joint specimens of the epoxy adhesive. Data are taken from table 4.

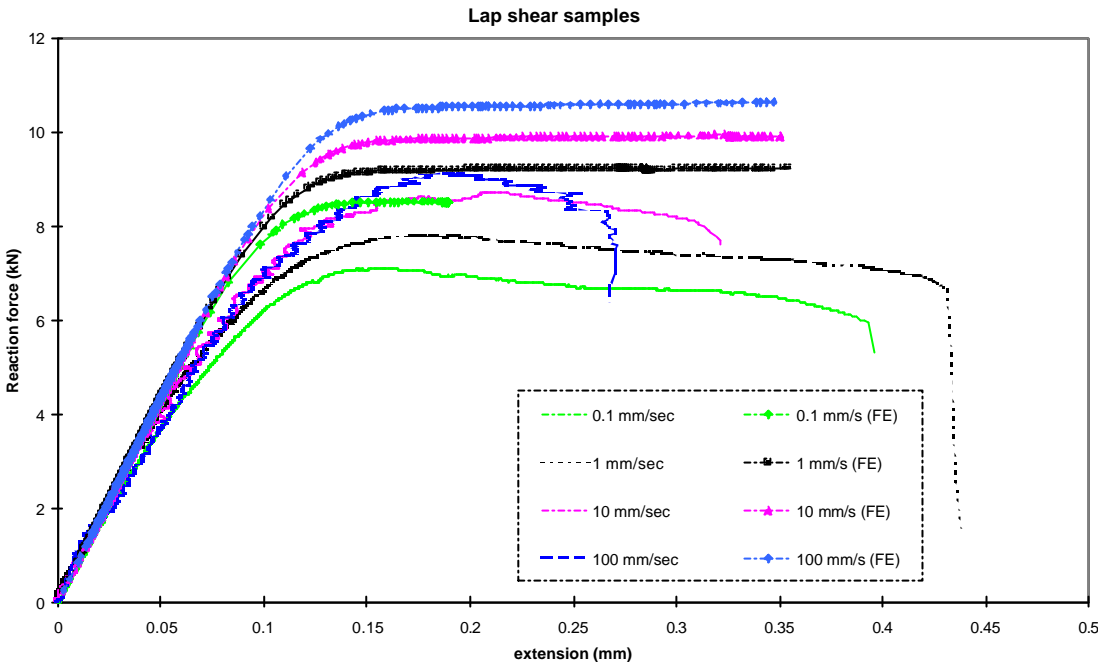


Figure 21. Comparison of predicted force/extension curves of lap-joint specimens at different loading speeds with measurements made using controlled displacement rate tests.

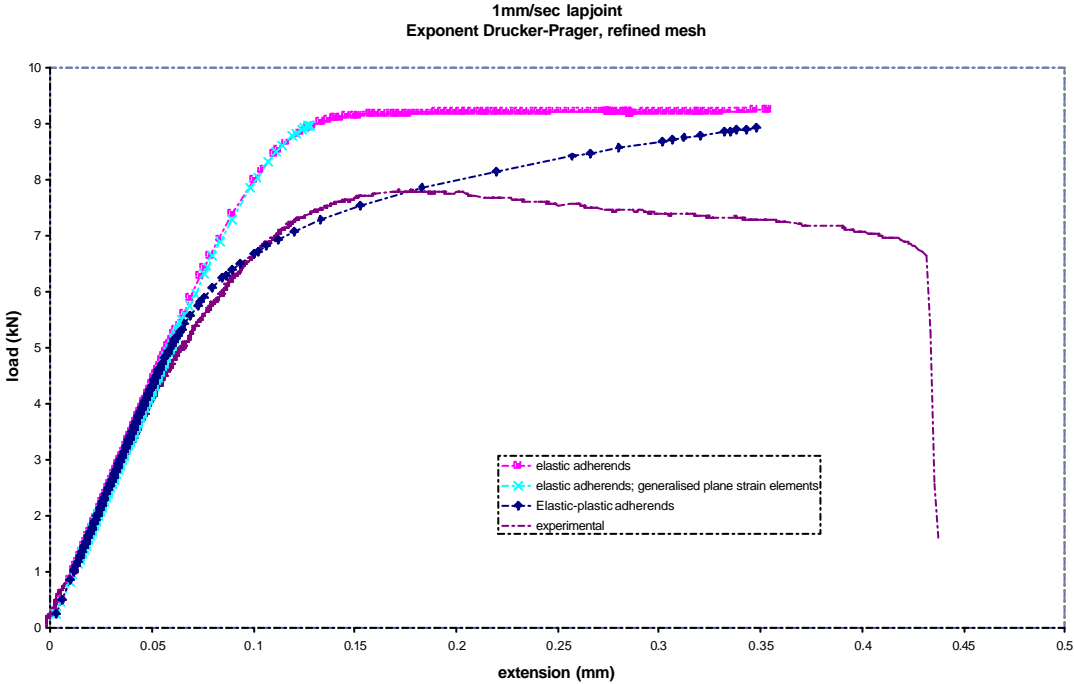


Figure 22. Force/extension curves at a speed of 1 mm/s comparing results of analyses obtained for plasticity in the steel adherends and generalised plane strain elements.

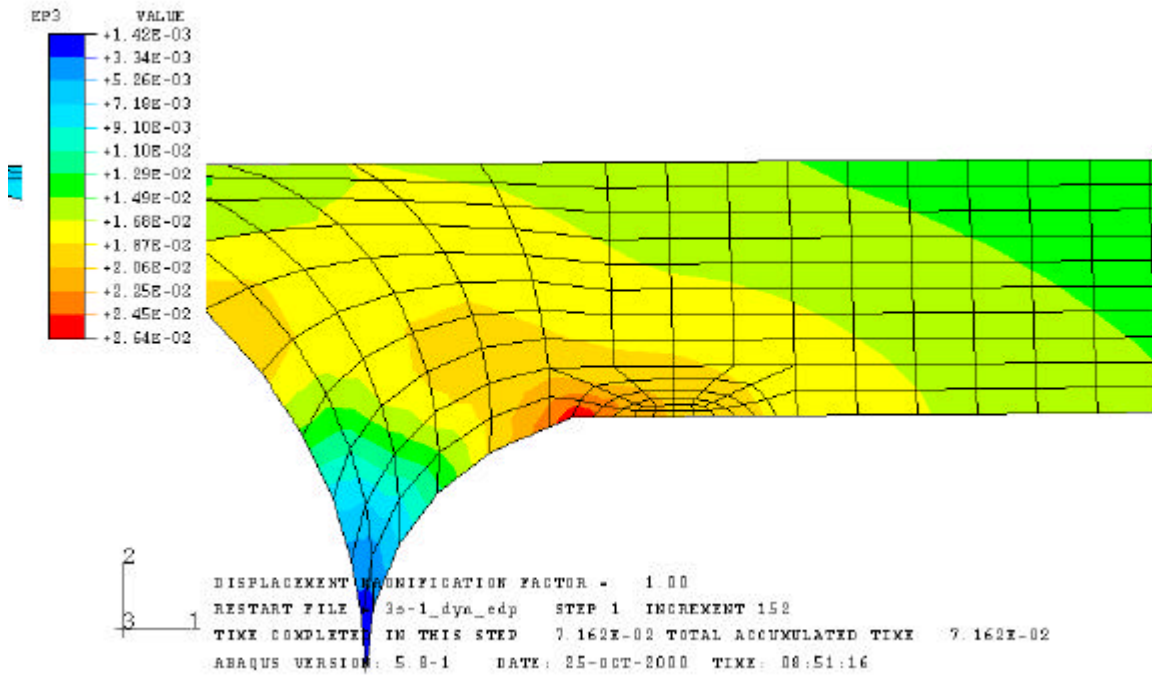


Figure 23. Calculated distribution of the maximum principle strain in the lap-joint at 0.05 mm extension.

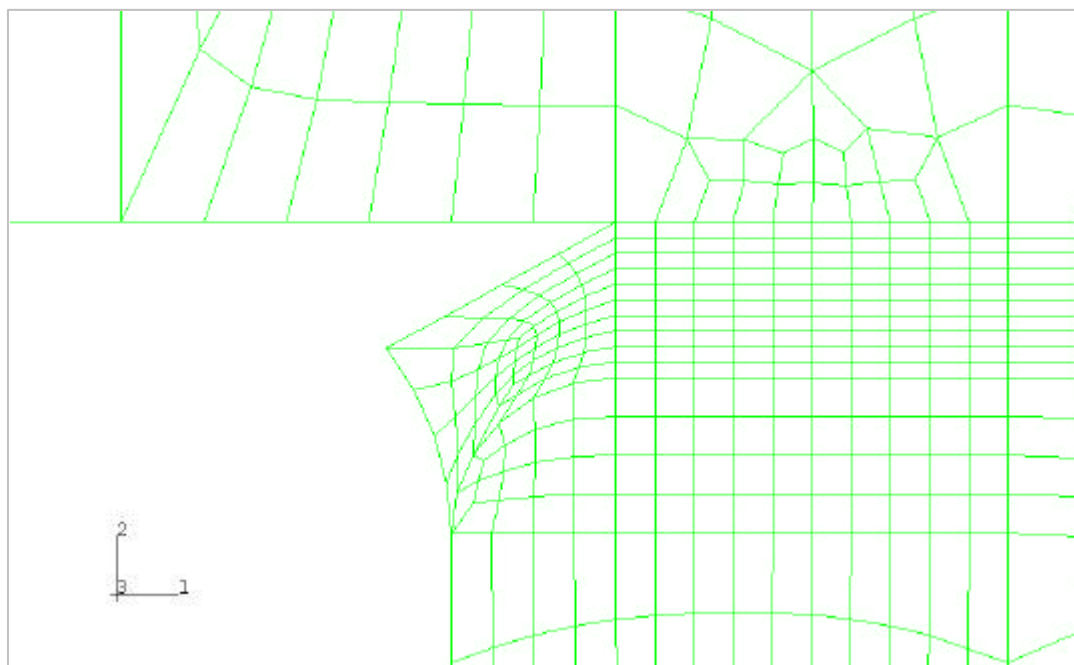


Figure 24. The mesh used to obtain predictions for a lap-joint specimen after partial rupture in the fillet region.

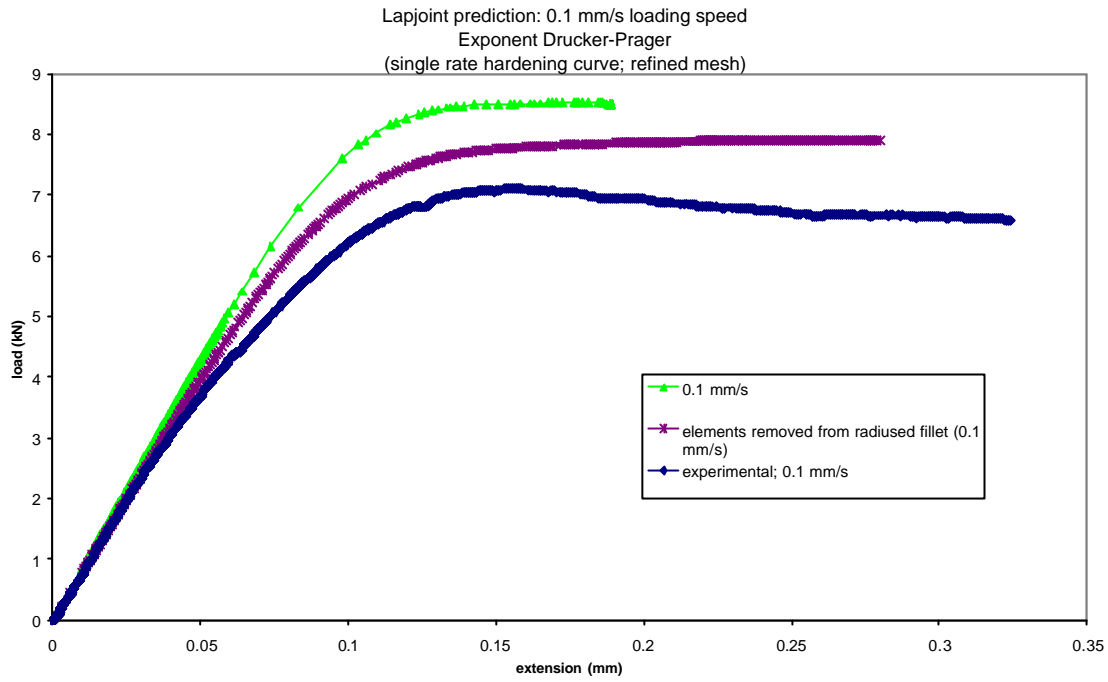


Figure 25. Comparison of force/extension curves for the complete and partially ruptured lap-joint with experimental data at 0.1 mm/s. Exponent Drucker-Prager model with single hardening curve at a strain rate of 0.3 s⁻¹.

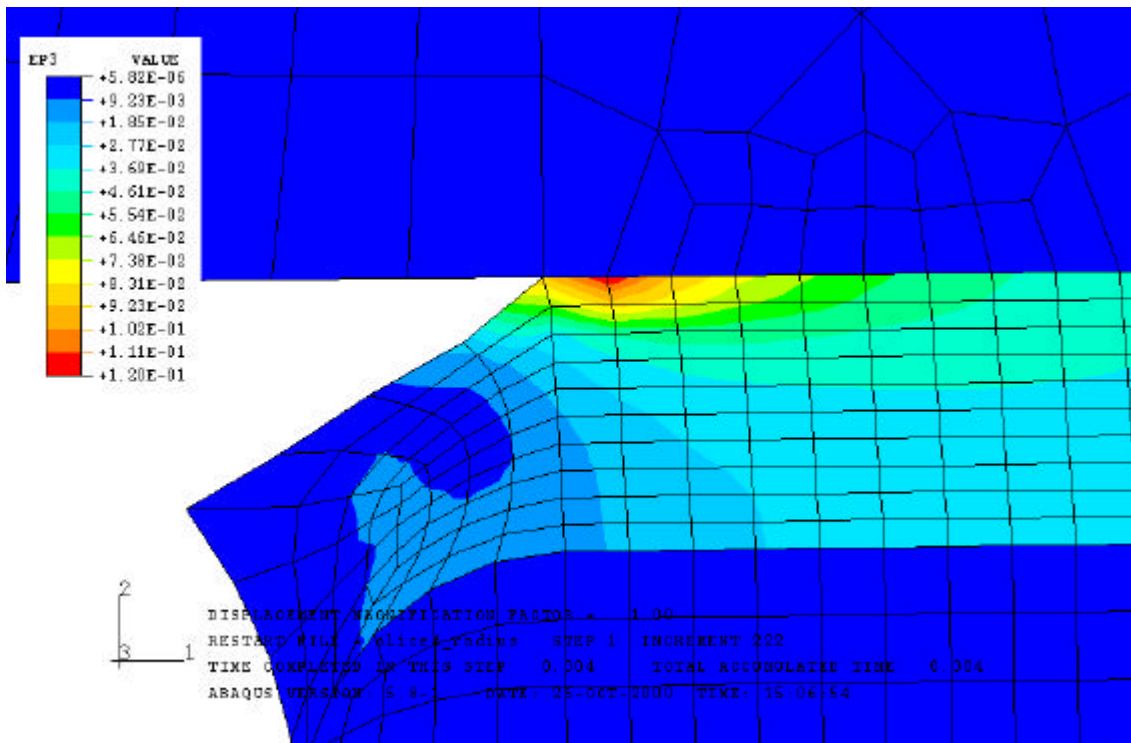


Figure 26. Distribution of the maximum principle strain in the lap-joint at 0.1 mm extension following the onset of rupture in the fillet.